Designing artificial cells to harness the biological ion concentration gradient

JIAN XU[1] AND DAVID A. LAVAN[2]*

[1]Department of Chemical Engineering, Yale University, New Haven, Connecticut 06520, USA
[2]National Institute of Standards and Technology, Gaithersburg, Maryland 20899, USA
*e-mail: david.lavan@nist.gov

Published online: 21 September 2008; doi:10.1038/nnano.2008.274

Cell membranes contain numerous nanoscale conductors in the form of ion channels and ion pumps[1–4] that work together to form ion concentration gradients across the membrane to trigger the release of an action potential[1,5]. It seems natural to ask if artificial cells can be built to use ion transport as effectively as natural cells. Here we report a mathematical calculation of the conversion of ion concentration gradients into action potentials across different nanoscale conductors in a model electrogenic cell (electrocyte) of an electric eel. Using the parameters extracted from the numerical model, we designed an artificial cell based on an optimized selection of conductors. The resulting cell is similar to the electrocyte but has higher power output density and greater energy conversion efficiency. We suggest methods for producing these artificial cells that could potentially be used to power medical implants and other tiny devices.

The electrocyte in an electric eel (*Electrophorus electricus*) can generate potentials of ~600 V (refs 2, 3 and 6) to stun prey and ward off predators (Fig. 1a). The transmembrane proteins in the electrocytes are asymmetrically distributed across two primary membranes, one innervated and the other non-innervated (Fig. 1b), and are separated by an insulating septa (wall). The non-innervated membrane has numerous sodium potassium ATPase pumps (Na^+/K^+) and both K^+ and chloride (Cl^-) channels. The innervated membrane contains high densities of acetylcholine receptors (AChRs), voltage-gated Na^+ channels (which are responsible for activating action potentials), voltage-gated K^+ channels (Kvs)[7], inward rectifier K^+ channels (Kirs, which are ion channels that stop ion flow when the membrane is depolarized)[6] and leak channels.

When the chemical agonist, acetylcholine (ACh), is released into the junction between the AChR and another nearby excitable cell (synapse), indicated by dots in Fig. 1b,c, AChRs bind with ACh and become permeable to the cations Na^+ and K^+. This opens the AChRs and depolarizes the innervated membrane, raising the probability that voltage-gated Na^+ channels will open (Fig. 1c)[3,6,8]. Depolarization causes the normally negative innervated cell membrane potential to become positive with respect to the potential on the non-innervated membrane. With Na^+ flowing into the cell, the innervated membrane potential further increases, causing the opening of additional voltage-gated Na^+ channels. This cascade of AChRs opening large numbers of Na^+ channels results in action potential formation on the innervated membrane. The Kir channels are closed during this stage, which speeds the increase of the membrane potential. The maximum innervated membrane potential is +65 mV (refs 5 and 6). The non-innervated membrane potential remains at ~−85 mV due to ATPase, K^+ channel and Cl^- activity[2,5,6]. After the peak of the action potential, the innervated membrane is repolarized with the inactivation of Na^+ channels[8] and the opening of Kir and Kv channels. Ion flux through leak channels further expedites the restoration of membrane potential to the resting state (−85 mV). The ion concentration gradient is sustained by Na^+/K^+-ATPase with energy obtained from the hydrolysis of the energy molecule, adenosine triphosphate (ATP)[9]. Ion flux, through the open ion channels, results in a net electric current from the innervated membrane to the non-innervated membrane.

Many mathematical models of axons have been produced, including the Hodgkin–Huxley model, which depicts the action potential formation on the squid giant axon (SGA) by ion transport through Na^+ channels, Kv and leak channels[1]; however, the natural electrocyte is more complicated as it is a polarized cell. Cell polarity is the necessary feature for directional transport and formation of transcellular potential[10]. Our model is based on cells arranged in series (Fig. 2a) powering an external circuit. In it, the innervated membrane is described by the Hodgkin–Huxley model, with additional current through Kirs and AChRs. The ion channels on the non-innervated membrane are described by the Goldman–Hodgkin–Katz current equation[8,11], which depicts the ion flux as a function of membrane potential and the transmembrane ion gradient. To compare the performance of different types of cells, we constructed a pseudo squid giant axon (PSGA) model from the known characteristics of the SGA and a generic model for the non-innervated membrane (this model is referred to as 'pseudo' because the SGA is not a polarized cell). (See Supplementary Information for detailed equations and parameters.)

Many electrophysiological parameters for the natural electrocyte, such as the channel rate constants and densities, are unknown or span a broad range[12,13]. We found accurate values for these parameters numerically by using a nonlinear least-squares difference method to match initial model results with the nuances of the rise and fall of action potential in published electrocyte data[5] (Fig. 2b). The ion channel configuration of the innervated membrane extracted from the action potential curve using this method is shown in Table 1; other physiological parameters, including the channel rate constants and the ion transporter configuration of the non-innervated membrane, were analysed (see Supplementary Information). In the model, the

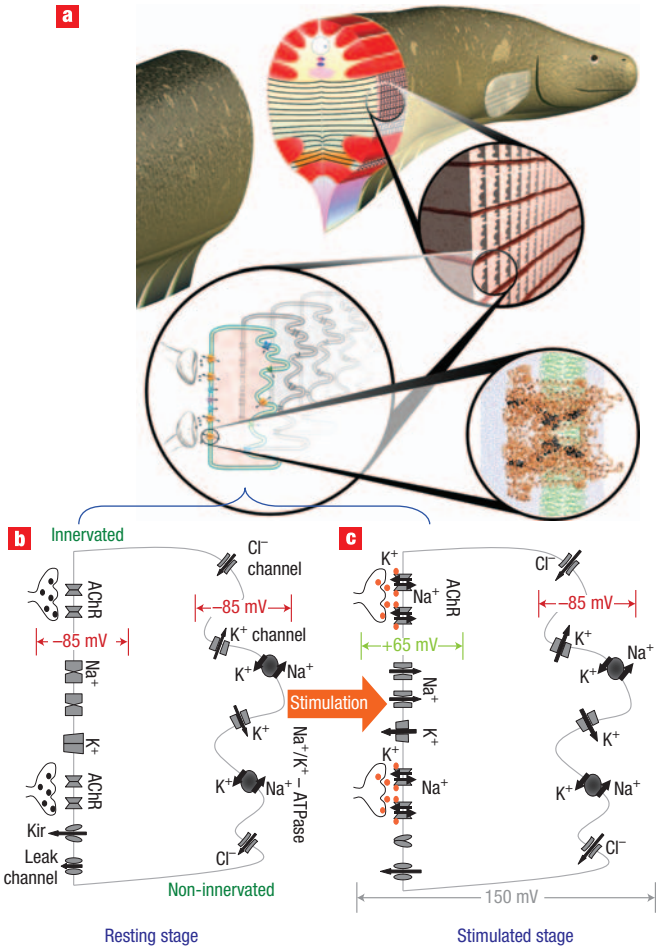

Figure 1 Anatomy of the electric eel and structure of the natural electrocyte. a, The anatomy of the electric eel. **b**,**c**, The electrocyte in the resting stage (**b**) and stimulated stage (**c**). See main text for details of the mechanism. Adapted from ref. 6.

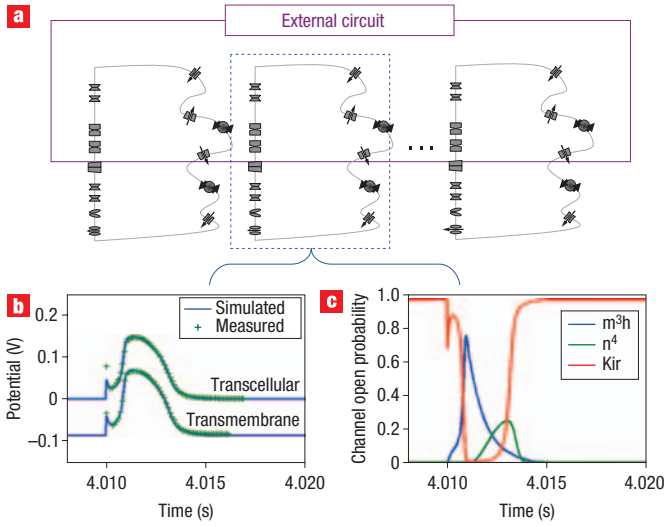

Figure 2 Schematic diagram of a system of electrogenic cells used in the simulations, and subsequent action potential formation. a, Multiple cells connected in series to drive an external circuit. **b**, Innervated membrane potential and transcellular potential from simulations (27 °C, data shown at 4.01 s) and recordings from a natural electrocyte[5]. **c**, Regression results for Na^+ (m^3h), Kv (n^4) and Kir channel open probability parameters for the innervated membrane.

conductance of Na^+ channels on the innervated membrane was found to be 1.57×10^3 pS μm^{-2}, equivalent to a channel density of ~143 channels μm^{-2}, which falls between the reported values of ~100 channels μm^{-2} (refs 12 and 13) and ~500 channels μm^{-2} (ref. 13). The innervated membrane capacitance was found to be 12.1 $\mu F\ cm^{-2}$, which has been experimentally reported as 15.6 $\mu F\ cm^{-2}$ (ref. 5); this high capacitance can be due to high local tortuosity or modification to the lipid[5,14]. The derived resting resistance, 16.3 $\Omega\ cm^2$, is also consistent with experimental data[2,5]. The model results for channel opening and closing sequences (Fig. 2c) are also in agreement with observations from the natural electrocyte[6,8].

As is well known for normal voltaic batteries, the voltage output of our model cell decreases when the external resistance (R) decreases (Fig. 3b), influencing the single pulse energy output (W_s). The dependence of energy output W_s on external resistance has been reported phenomenologically[15,16]. The cell has maximum W_s when the voltage output is approximately half of the open-circuit voltage.

The energy output of the artificial cell was optimized numerically (Table 1). The design started as a list of nanoconductors (channels and pumps), basic physical parameters (two membranes, known ion permeability, and so on) and a mathematical equation, known as an objective function, which quantifies the desired criteria (that is, energy output or energy density). Numerical methods are used to impartially maximize the value of the objective function given the starting parameters, equations and constraints. The output is the configuration for an artificial cell that maximizes the value of the objective function. Constrained nonlinear numerical optimization was used to guide the parametric design for the artificial cell. One constraint was to maintain the overall channel number as a constant on each membrane; the numbers of individual types of ion channels were varied in the optimization algorithm. The resulting artificial cell, with the same total channel/pump density as the natural electrocyte, produces 41% more energy per pulse (Table 1), with longer action potential duration (Fig. 3a). These results are based on the comparisons between the models of the artificial cell and the electrocyte. There are many small differences between the model and true physical behaviour; however, comparing the results of the models eliminates this error.

The power output of a cell is affected by both R and the stimulus interval. At any given R, the cell produces maximum power output (P) when it is excited at an interval slightly longer than the refractory period (the time taken to be ready for another action potential) plus the action potential duration (Fig. 4a). The natural electrocyte has a peak power output of 0.427 $W\ m^{-2}$, and one PSGA produces only 0.0233 $W\ m^{-2}$. One artificial cell can produce 0.545 $W\ m^{-2}$ (Table 1); without increasing channel or pump density, the peak power output for the artificial cell surpasses the natural electrocyte by 28%.

The transmembrane ion gradient of the cell is sustained by Na^+/K^+-ATPases, which are fuelled by ATP hydrolysis[9] using the energy from the oxidization of glucose or fatty acids[17]. In our model the natural electrocyte has an energy conversion efficiency of 14.7%; it has been reported experimentally to be 15.4%[15]. The PSGA converts energy more efficiently (19.7%) than the electrocyte, but

Table 1 Performance and parameters of natural, simplest and artificial cells. Channel configurations for each design are shown, along with peak values for single pulse energy output, maximum power output and maximum energy conversion efficiency.

		Natural electrocyte	PSGA	Simplest cell	Artificial cell	Artificial cell/ electrocyte (%)
Channel conductance, g (S m^{-2})	Na^+	1.57×10^3	1.20×10^3	7.87×10^2	2.18×10^3	139
	Kv	3.20×10^2	3.60×10^2	0	0	0
	Leak	3.43×10^1	3.00	2.40×10^2*	2.78×10^1	81
	Kir	5.91×10^2	0	0	4.78×10^2	81
Single pulse energy output	$W_{s,peak}$ (J m^{-2} pulse^{-1} cell^{-1})	2.13×10^{-3}	3.68×10^{-5}	3.77×10^{-4}	3.02×10^{-3}	141†
Maximum power output	P_{peak} (W m^{-2} cell^{-1})	0.427	0.023	0.014	0.545	128†
Maximum energy conversion efficiency (%)	C_{peak}	14.7	19.7	3.86	19.2	131†

* Includes a K^+ leak channel that is not found in the natural electrocyte or artificial cell.
†Configurations with higher energy or power output.

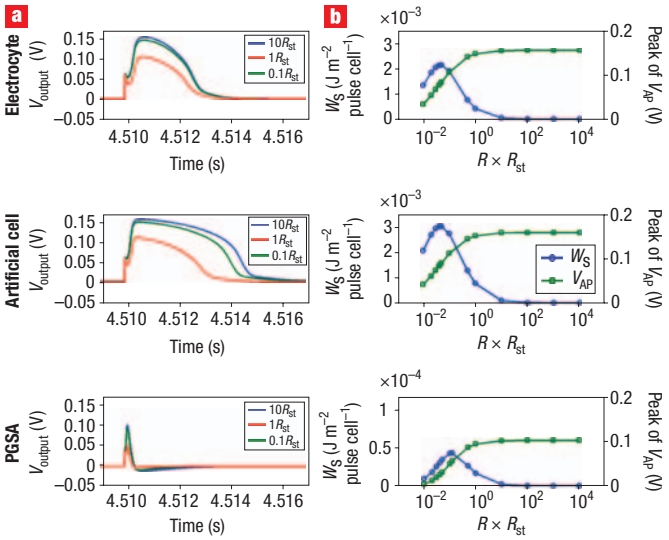

Figure 3 A comparison of action potentials formed in the electrocyte, artificial cell and pseudo squid giant axon. The action potentials for the artificial cell are based on maximizing the single pulse energy output. **a**, Transcellular potential of the electrocyte as a function of external resistance, R. **b**, Peak of transcellular voltage output V_{AP} and single pulse energy output W_s as a function of R. (R normalized to $R_{st} = 8.53 \times 10^{-2}\ \Omega\ m^2\ cell^{-1}$, ref. 5).

the SGA serves a different function and the natural SGA and PSGA models have different electrophysiological parameters (such as unitary conductances) from the electrocyte. The peak efficiency of the artificial cell was found to be 19.2% (Table 1).

Our numerical optimization of the cell design has produced the design for an artificial cell with both higher power output density and greater energy conversion efficiency than the natural electrocyte. The lack of voltage-gated K^+ channels in the artificial cell (Table 1) is consistent with the understanding of their function to shorten the action potential duration. The action potential from the PSGA has a smaller amplitude, shorter duration and shorter refractory period. These differences are well suited to its role—to conduct nerve pulses at high speed with little energy use. The electrocyte must generate large pulses less frequently to shock prey and defend against predators; its action potential has a broader duration and higher amplitude. The action potential of the artificial cell has even longer duration.

The reported configurations all fall into a stable excitable region, where at most one action potential is elicited by one stimulus. Intrinsic in the model is a regime in which the cell oscillates (repetitive firings of action potentials without recurring stimuli). In this regime, even at the resting potential, the inward sodium current through the Na^+ channels exceeds the outward current through the Kir and leak channels, which depolarizes the membrane, makes the sodium current regenerative and forms repetitive action potentials. As both power output and energy conversion efficiency are lower in this regime, it was not included in the optimization.

Each artificial cell can produce 0.545 W m^{-2}. The power output density of cells in series would scale linearly with the number of layers. A power of 300 μW could be produced continuously with a device of dimensions 4.3 mm × 4.3 mm × 3.9 mm, with a channel density on the innervated membrane of ~350 channels μm^{-2}. It may be possible to increase this power density further given more than fivefold higher channel density measurements in other cells[8,18]; however, the maximum energy conversion efficiency is most dependent on the performance of individual channels and the ratio of different channel types rather than the overall channel density. The artificial cell would be able to supply electrical energy for powering medical implants, including retinal prostheses[19]. The supply of ATP can be sustained either by coupling a proton-gradient-driven F_oF_1-ATPase with a light-driven proton pump such as bacteriorhodopsin[20], or by inserting isolated mitochondria[21] or bacteria[22] into the artificial cell. The model was also used to find the simplest cell capable of generating an action potential from an electrical stimulus; the simplest cell requires voltage-gated Na^+ channels and K^+ leak channels on the innervated membrane and both Kv channels and Na^+/K^+-ATPases on the non-innervated membrane. The performance of the simplest cell is substantially lower than the electrocyte or the artificial cell (Table 1).

The artificial cell would consist of two artificial cell membranes (mimicking innervated and non-innervated membranes) separating aqueous solutions. Supported bilayers can maintain the function of inserted ion transporters[23]; each membrane could be a supported lipid bilayer on a porous structure, such as mesoporous silica[24]. Many natural ion channels can be purified by affinity chromatography and inserted into lipid bilayers by vesicle fusion[25,26]. The numbers of inserted ion channels/pumps can be monitored by measuring the membrane current during insertion. Artificial ion channels might be made by precisely tailoring the pore size of SiO_2 nanopores using approaches such as TiO_2 atomic layer deposition[27] and organic group functionalization[28]. Synthetic channels can also be engineered using α-haemolysin (α-HL); their properties (for example, unitary conductance, gating and ion selectivity) can be tailored by protein or chemical engineering[29]. Artificial channels may also be synthesized from peptides or other molecules[30]. These artificial channels can mimic natural channels

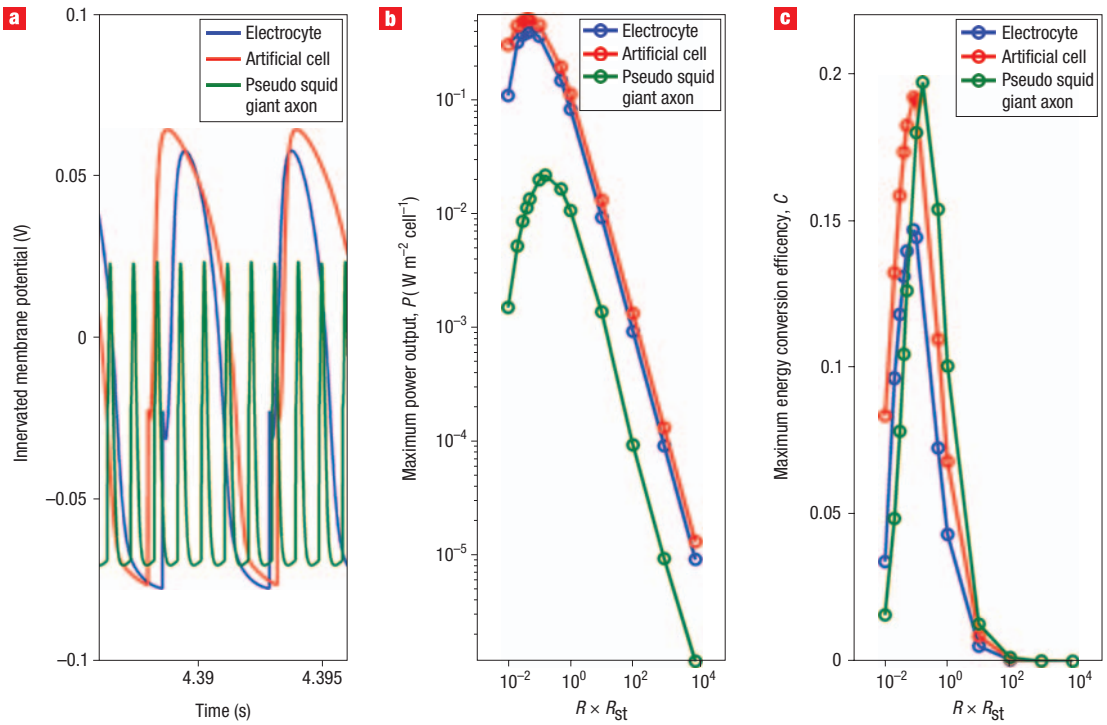

Figure 4 A comparison of action potentials formed in the electrocyte, artificial cell and pseudo squid giant axon. The action potentials for the artificial cell are based on maximizing the power output and energy conversion efficiency over many seconds. **a**, Action potential formation when the cells are stimulated at the optimal interval (external resistance $R = R_{st}$, 27 °C, stimulus: −21.3 mV). **b**, Maximum power output P as a function of R. **c**, Maximum energy conversion efficiency C as a function of R.

and may offer enhanced stability and tailored electrophysiology. The artificial cells would be connected in series, to increase the total voltage output, or in parallel, to raise the current output. A number of layered cells could be fired by injecting current at the top or bottom of the stack.

It is interesting to note that this work has mapped out changes in the system-level design of the electrocyte that could produce higher energy density and convert energy more efficiently. These changes may show the next step in the evolution of these cells; it is also possible that there are advantages to the species in maintaining this lower energy conversion efficiency.

METHODS

Models were written in MATLAB 7.5 (The Mathworks) running under a 64-bit operating system (Windows Server 2003, Microsoft Corporation) on a multiprocessor server with 8 GB of RAM. Unknown channel parameters were extracted by matching published experimental data to the model using regression methods. Once the natural channel parameters were found, the parametric design inputs for the model were varied using a nonlinear optimization algorithm to search for the optimal configuration of the artificial cell to maximize the objective functions. Objective functions are the mathematical relationships that quantify the 'goodness' of the design, such as the energy conversion efficiency or the energy density of the devices. The optimization algorithm would vary the design parameters and calculate the formation of many action potentials until steady-state conditions were reached; at that point the objective function would be evaluated and the optimization routine would compare the current value of the objective function to previous values and decide to either stop the optimization (if a maximum was reached) or vary additional parameters in an effort to further maximize the objective function.

Received 5 May 2008; accepted 19 August 2008; published 21 September 2008.

References

1. Hodgkin, A. & Huxley, A. A quantitative description of membrane current and its application to conduction and excitation in nerve. *J. Physiol.* **117,** 500–544 (1952).
2. Altamirano, M. Electrical properties of the innervated membrane of the electroplax of electric eel. *J. Cell. Physiol.* **46,** 249–277 (1955).
3. Mermelstein, C., Costa, M. & Neto, V. The cytoskeleton of the electric tissue of *Electrophorus electricus*, L.*. *Ann. Acad. Bras. Cienc.* **72,** 341–351 (2000).
4. Rosenberg, R. L., Tomiko, S. A. & Agnew, W. S. Single-channel properties of the reconstituted voltage-regulated Na channel isolated from the electroplax of *Electrophorus electricus*. *Proc. Natl Acad. Sci. USA* **81,** 5594–5598 (1984).
5. Keynes, R. & Ferreira, H. Membrane potentials in the electroplates of the electric eel. *J. Physiol.* **119,** 315–351 (1953).
6. Gotter, A., Kaetzel, M. & Dedman, J. *Electrophorus electricus* as a model system for the study of membrane excitability. *Comp. Biochem. Physiol.* **119A,** 225–241 (1998).
7. Thornhill, W. B. *et al.* Molecular cloning and expression of a Kv1.1-like potassium channel from the electric organ of *Electrophorus electricus*. *J. Membr. Biol.* **196,** 1–8 (2003).
8. Hille, B. *Ion Channels of Excitable Membranes* 3rd edn (Sinauer Associates, Sunderland, MA, 2001).
9. Tanford, C. Equilibrium state of ATP-driven ion pumps in relation to physiological ion concentration gradients. *J. Gen. Physiol.* **77,** 223–229 (1981).
10. Ussing, H. H. The frog skin potential. *J. Gen. Physiol.* **43,** 135–147 (1960).
11. Novotny, J. & Jakobsson, E. Computational studies of ion-water flux coupling in the airway epithelium. I. Construction of model. *Am. J. Physiol.* **270,** C1751–C1763 (1996).
12. Shenkel, S. & Bezanilla, F. Patch recordings from the electrocytes of electrophorus. Na channel gating currents. *J. Gen. Physiol.* **98,** 465–478 (1991).
13. Shenkel, S. & Sigworth, F. Patch recordings from the electrocytes of *Electrophorus electricus*: Na Currents and P_{Na}/P_K variability. *J. Gen. Physiol.* **97,** 1013–1041 (1991).
14. Dilger, J. P., McLaughlin, S. G., McIntosh, T. J. & Simon, S. A. The dielectric constant of phospholipid bilayers and the permeability of membranes to ions. *Science* **206,** 1196–1198 (1979).
15. Cox, R. T., Coates, C. W. & Brown, M. V. Electric tissue—relations between the structure, electrical characteristics, and chemical processes of electric tissue. *J. Gen. Physiol.* **28,** 187–212 (1945).
16. Nachmansohn, D., Cox, R. T., Coates, C. W. & Machado, A. L. Action potential and enzyme activity in the electric organ of *Electrophorus electricus*. ii. Phosphocreatine as energy source of the action potential. *J. Neurophysiol.* **6,** 383–396 (1943).
17. Berg, J., Tymoczko, J. & Stryer, L. Biochemistry (W. H. Freeman and Company, New York, 2001).
18. Conti, F., Hille, B., Neumcke, B., Nonner, W. & Stampfli, R. Measurement of the conductance of the sodium channel from current fluctuations at the node of Ranvier. *J. Physiol.* **262,** 699–727 (1976).
19. Humayun, M. *et al.* Visual perception in a blind subject with a chronic microelectronic retinal prosthesis. *Vision Res.* **43,** 2573–2581 (2002).
20. Yrach, G. *et al.* Light-driven production of ATP catalysed by F_oF_1-ATP synthase in an artificial photosynthetic membrane. *Nature* **392,** 479–482 (1998).
21. Drew, B. & Leeuwenburgh, C. Method for measuring ATP production in isolated mitochondria: ATP production in brain and liver mitochondria of Fischer-344 rats with age and caloric restriction. *Am. J. Physiol.: Regul. Integr. Comp. Physiol.* **285,** R1259–R1267 (2005).

22. Maloney, P. C., Kashket, E. R. & Wilson, T. H. A protonmotive force drives ATP synthesis in bacteria. *Proc. Natl Acad. Sci. USA* **71,** 3896–3900 (1974).
23. Romer, W. & Steinem, C. Impedance analysis and single-channel recordings on nano-black lipid membranes based on porous alumina. *Biophys. J.* **86,** 955–965 (2004).
24. Brinker, J., Lu, Y., Sellinger, A. & Fan, H. Evaporation-induced self-assembly: nanostructures made easy. *Adv. Mater.* **11,** 579–585 (1999).
25. Hanke, W. & Schlue, W. *Planar Lipid Bilayers: Methods and Applications* (Academic Press, San Diego, 1993).
26. Recio-Pinto, E., Duch, D., Levinson, S. & Urban, B. W. Purified and unpurified sodium channels from eel electroplax in planar lipid bilayers. *J. Gen. Physiol.* **90,** 375–395 (1987).
27. Jiang, Y.-B. *et al.* Sub-10 nm thick microporous membranes made by plasma-defined atomic layer deposition of a bridged silsesquioxane precursor. *J. Am. Chem. Soc.* **129,** 15446–15447 (2007).
28. Liu, N., Assink, R. A. & Brinker, C. J. Synthesis and characterization of highly ordered mesoporous thin films with –COOH terminated pore surfaces. *Chem. Commun.* 370–371 (2003).
29. Merzlyak, P. G., Capistrano, M. F. P., Valeva, A., Kasianowicz, J. J. & Krasilnikov, O. V. Conductance and ion selectivity of a mesoscopic protein nanopore probed with cysteine scanning mutagenesis. *Biophys. J.* **89,** 3059–3070 (2005).
30. Matile, S., Som, A. & Sord, N. Recent synthetic ion channels and pores. *Tetrahedron* **60,** 6405–6435 (2004).

Supplementary Information accompanies this paper at www.nature.com/naturenanotechnology.

Acknowledgements

We thank F. Sigworth, E. Jakobsson, S. Natarajan, J. Novotny, T.P. Ma and S. Yulke for their discussions and comments. The full description of the procedures used in this paper requires the identification of certain software and operating systems and their suppliers. The inclusion of such information should in no way be construed as indicating that such software or operating systems are endorsed by NIST or are recommended by NIST or that it is necessarily the best software or operating system for the purposes described. This work is supported by the National Centre for Design of Biomimetic Nanoconductors, funded by grant no. PHS 2 PN2 EY016570B from the National Institutes of Health through the NIH Roadmap for Medical Research.

Author contributions

J.X. and D.A.L. conceived and designed the experiments. J.X. performed the experiments. J.X. and D.A.L. analysed the data and co-wrote the paper.

Author information

Reprints and permission information is available online at http://npg.nature.com/reprintsandpermissions/.
Correspondence and requests for materials should be addressed to D.A.L.